processes

MDPI

Article

The Calcium Channel Affect Osteogenic Differentiation of Mesenchymal Stem Cells on Strontium-Substituted Calcium Silicate/Poly-ε-Caprolactone Scaffold

Tzu-Rong Su [1,†], Tsui-Hsien Huang [2,3,†], Chia-Tze Kao [2,3], Hooi Yee Ng [4,5], Yung-Cheng Chiu [4,*] and Tuan-Ti Hsu [6,*]

1 Department of Dentistry, Antai Medical Care Cooperation Antai Tian-Sheng Memorial Hospital, Pingtung 928, Taiwan; a081002@mail.tsmh.org.tw
2 School of Dentistry, Chung Shan Medical University, Taichung City 402, Taiwan; thh@csmu.edu.tw (T.-H.H.); ctk@csmu.edu.tw (C.-T.K.)
3 Department of Stomatology, Chung Shan Medical University Hospital, Taichung City 402, Taiwan
4 School of Medicine, China Medical University, Taichung City 402, Taiwan; hooiyeen@gmail.com
5 Department of Orthopedic Surgery, China Medical University Hospital, Taichung 402, Taiwan
6 3D Printing Medical Research Center, China Medical University Hospital, Taichung City 402, Taiwan
* Correspondence: ycchiu@me.com (Y.-C.C.); nakohsu@gmail.com (T.-T.H.); Tel.: +886-4-22052121 (T.-T.H.); Fax: +886-4-24759065 (T.-T.H.)
† These authors contributed equally to this work.

Received: 5 January 2020; Accepted: 2 February 2020; Published: 6 February 2020

Abstract: There had been a paradigm shift in tissue engineering studies over the past decades. Of which, part of the hype in such studies was based on exploring for novel biomaterials to enhance regeneration. Strontium ions have been reported by others to have a unique effect on osteogenesis. Both in vitro and in vivo studies had demonstrated that strontium ions were able to promote osteoblast growth, and yet at the same time, inhibit the formation of osteoclasts. Strontium is thus considered an important biomaterial in the field of bone tissue engineering. In this study, we developed a Strontium-calcium silicate scaffold using 3D printing technology and evaluated for its cellular proliferation capabilities by assessing for protein quantification and mineralization of Wharton's Jelly mesenchymal stem cells. In addition, verapamil (an L-type of calcium channel blocker, CCB) was used to determine the mechanism of action of strontium ions. The results found that the relative cell proliferation rate on the scaffold was increased between 20% to 60% within 7 days of culture, while the CCB group only had up to approximately 10% proliferation as compared with the control specimen. Besides, the CCB group had downregulation and down expressions of all downstream cell signaling proteins (ERK and P38) and osteogenic-related protein (Col I, OPN, and OC). Furthermore, CCB was found to have 3–4 times lesser calcium deposition and quantification after 7 and 14 days of culture. These results effectively show that the 3D printed strontium-contained scaffold could effectively stimulate stem cells to undergo bone differentiation via activation of L-type calcium channels. Such results showed that strontium-calcium silicate scaffolds have high development potential for bone tissue engineering.

Keywords: calcium channel blocker; verapamil; strontium; osteogenic; 3D printing

1. Introduction

Large bone defects caused by trauma, tumor, and age-related bone diseases can be troubling for surgeons as there are currently no appropriate treatments to allow complete recovery [1]. Furthermore,

the prevalence of the aging population in developed and developing countries is forecasted to increase over the next few decades; thus, the incidence of diseases causing large bone defects such as osteoporosis is bound to increase. The most promising treatment methodology currently is bone grafting. However, issues like immunological rejections, lack of suitable grafting sources and lengthened surgical durations are some of the problems waiting to be solved in bone grafting surgeries [2]. Therefore, to tackle this imminent problem, scientists have since attempted to find viable bone substitutes that have greater regeneration capabilities for large bone defects [3,4]. With the emergence of 3D printing technologies, tissue engineering researchers are now attempting to find suiTable 3D printable biomaterials for the fabrication of potential bone substitutes [5–7]. 3D printing technology is a process that allows for the rapid manufacturing of 3D designed structures designed with computer-assisted design software [8]. In addition, with the assistance of the 3D printing process, it is possible to design personalized bone grafts that have specific structures and morphology to suit a patient's needs [9]. Currently, 3D printed bone substitutes and grafts have lesser governing regulations as they are currently noted to have lower risks as compared to the traditional method of using osteoinduction [10,11].

Calcium silicate (CS) ceramics had attractive properties such as having the capability to induce enhanced, enhanced osteoconductivity, and the ability to have in-vivo biodegradation [12]. Amongst all the available biomaterials in the market, CS-based ceramics are a widely studied biomaterial for bone bioengineering due to their potential in osteoinduction and excellent biocompatibility [13]. CS-based ceramics are widely reported to have the abovementioned characteristics due to their ability to constantly and steadily release Si ions into its environment [14]. Of which, certain amounts of Si in the micro-environment are reported to enhance cellular adhesion, proliferation and subsequent downstream activities such as osteogenesis [15]. In addition, Si ion has also been reported to be involved in up-regulating expressions of angiogenic factors [16]. Furthermore, phosphate ions in simulated body fluid (SBF) have been shown to react with Ca ion on the surface of CS scaffolds to form hydroxyapatite mineralization on the surfaces. Such mineralization allows the surface to become hydrophilic which then enhances tissue binding capability of the scaffold onto live tissues. In addition, several studies had been conducted which concluded that the addition of metallic ions into biomaterials was able to upregulate cellular activities and increase biological and anti-inflammatory capabilities [12,17,18]. In our previous study, we successfully incorporated strontium (Sr) into CS powder and fabricated 3D SrCS scaffold contained suitable porosity via 3D printing methods and such a SrCS biomaterial was also shown to enhance bone regeneration by increasing osteogenesis and angiogenesis [19,20].

However, there is not much research to confirm how Sr actually affects cellular physiological behavior. Some researchers believe that Ca and Sr have identical in vivo characteristics [21]. In addition, Sr had garnered the attention of researches due to its "dual regulatory" properties, as it was found to be able to excite osteoblast to secrete new bone-related matrix protein and yet simultaneously reduce bone resorption by regulating the receptor activator of the nuclear factor κ-B ligand (RANK)/osteoprotegerin (OPG) signaling pathway. OPG is a decoy receptor to RANK; thus, when activated, it inhibits osteoclast activity in which Sr was shown to up-regulate OPG activation. Furthermore, Sr ions are also reported to be able to activate the mitogen-mediated protein kinase (MAPK) pathway, and regulate the calcium-dependent cellular signaling pathway through the Ca-sensing receptor (CaSR), which is a common physiological receptor for osteoblasts to increase cellular activities. However, the exact mechanisms behind such capabilities of SrCS scaffolds are still not well studied or understood.

The aim of this study was to explore the effects that a 3D-printed SrCS scaffold has on human Wharton's jelly mesenchymal stem cells (WJMSC) when the cells are seeded onto the scaffolds. Osteogenic related proteins and proliferation markers were assessed in this study. In addition, an L-type calcium channel blocker, verapamil, was applied to the cell culture order to examine the mechanisms behind such enhancements. In conclusion, this study showed that SrCS scaffolds were able to manipulate sequential molecular events through Ca-channels which in turn promote cellular behaviors and activities such as enhancing ERK/MAPK for osteogenic differentiation.

2. Results

2.1. Scaffold Fabrication

Printed SrCS scaffolds were shown in Figure 1A. From the images, it can be noted that the scaffolds had smooth and continuous surfaces and edges, thus strongly suggesting that Sr modification does not affect the quality of 3D extrusion printing. The size and shapes of the printed products were similar to our design of a 6.5 × 6.5 × 10 mm square shape with 500 µm pores between the struts. As seen from the images, the square pores of the scaffolds were obvious and constant and the corners of the pores were located approximately 90º to the struts. In addition, the ends of the struts were not blunt or extended, thus showing that the printing breaks and quality were not affected by the addition of Sr. The different layers of the struts were able to stack with one another without collapsing. The X-ray diffraction (XRD) analysis indicated the SrCS scaffold had diffraction peaks at 33.5°, 33.8°, and various peaks between 38.7° to 42.8° (Figure 1B). Furthermore, the existence of the various Sr peaks confirmed the successful incorporation of Sr into CS powders [19].

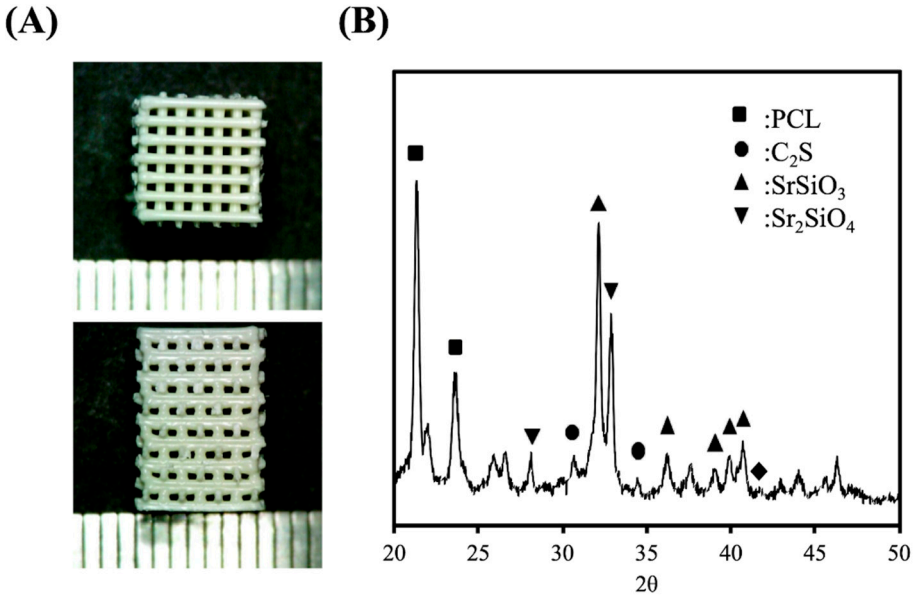

Figure 1. (**A**) Different view and (**B**) X-ray diffraction patterns of the 3D printed strontium calcium silicate (SrCS) scaffolds.

2.2. Immersion Behavior

After 30 days of immersion, the surfaces of the scaffolds were examined using SEM to assess the apatite formation capabilities of the various scaffolds. The results are shown in Figure 2A. As seen from the images, there was basically no precipitation formation at day 0. Instead, it can be seen that the surfaces of the SrCS scaffolds were irregular and rough with different levels of contours. However, the clusters of apatite precipitation were seen on the surfaces after 1 day of immersion. After immersion for 7 days, the surface of the scaffold was entirely covered with clusters of apatite precipitation. However, it can be noted that the precipitation was not even and was mainly in clusters. SEM images after 30 days of immersion showed that the surfaces of the scaffold were covered with a homogenous layer of hydroxyapatite crystals. In addition, XRD results also demonstrated SrCS scaffold had apatite precipitation after 1, 7 and 30 days of immersion, as shown in Figure 2B. It was noted that the intensity of both SrSiO3 and Sr2SiO4 peaks at 32.8° and 33.3° decreased slightly at day 7 as compared to day 1. However, on day 30, there was a significant decrease in the intensity of both peaks. On the other hand, there were no notable apatite compounds on days 1 and 7. However, on day 30, a strong presence of apatite could be noted at the 25.9° mark. The values of Ca, Si, and Sr ion concentrations of SrCS

after immersion in SBF for different durations are shown in Figure 3. It can be seen that there was a gradual decline of Ca ions with approximately 1.48 mM, 1.25 mM, and 1.04 mM at 1, 3, and 7 days of immersion, respectively. Si and Sr ions, on the other hand, had an initial burst release during the first day of immersion which declined to a gradual release for the next 6 days. The level of Si ions was approximately 0.95 mM, 1.42 mM and 1.77 mM at 1, 3, and 7 days of immersion, respectively whilst Sr ions were at 0.19 mM, 0.28 mM, and 0.50 mM at 1, 3, and 7 days of immersion, respectively.

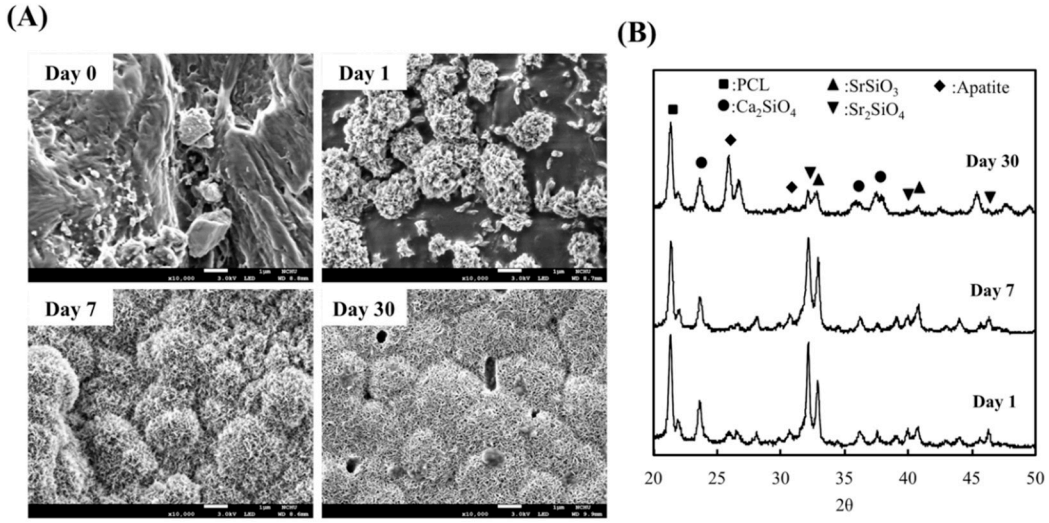

Figure 2. (**A**) SEM images of the surfaces of SrCS scaffolds and (**B**) X-ray diffraction patterns of SrCS scaffold after immersed in simulated body fluid (SBF).

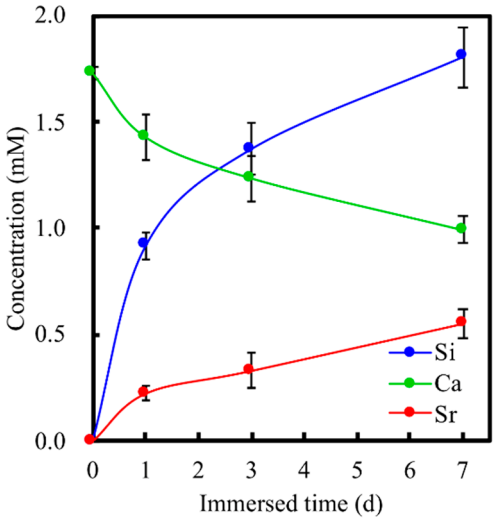

Figure 3. Ca, Si, and Sr ions concentrations in SBF after immersion for different durations. Data presented as mean ± SEM, $n = 6$ for each group.

2.3. Cell Proliferation

The proliferation of Wharton's Jelly mesenchymal stem cells (WJMSCs) cultured with the various groups and immunofluorescence images of WJMSCs cultured on SrCS is shown in Figure 4. As noted in Figure 4A, SrCS was able to significantly enhance the proliferation of WJMSCs as compared to control (Ctl) which was also in good agreement with reports made previously ($p < 0.05$). SrCS had approximately 1.2-, 1.4-, and 1.6-times the level of proliferation as compared to Ctl after 1, 3 and, 7 days of culture, respectively. It is worth noting that there was only a non-significant decrease in proliferation of the Ctl/ calcium channel blocker (CCB) group as compared to Ctl. However, all

groups had significant decreased proliferation as compared to SrCS. The differences between SrCS and SrCS/CCB were more significant than compared to Ctl, and Ctl/CCB. SrCS/CCB had approximately a 1.4x decrease in proliferation as compared to SrCS after 7 days of culture, whilst Ctl/CCB had only 1.1x decrease as compared to Ctl after similar culture durations. In addition, it was interesting to note that even with the effects of CCB, SrCS/CCB still had higher levels of proliferation as compared to Ctl and Ctl/CCB at all time points. Immunofluorescence was done to augment the quantitative proliferative results from Figure 4A. After 3 days of culture, cells from the SrCS group displayed a more flattened and elongated shape as compared to cells from the SrCS/CCB group. Several cells in the SrCS group had numerous extended cytoplasmic protrusions which could indicate ongoing mitosis. On the other hand, cells from the SrCS/CCB group were rounded, aggregated, and occupied lesser surface area as compared to SrCS. The immunofluorescence results from day 7 revealed similar features as described above. However, it could be clearly observed that there were higher quantities of cell nucleus and cells were well spread in the SrCS group as compared to the SrCS/CCB group.

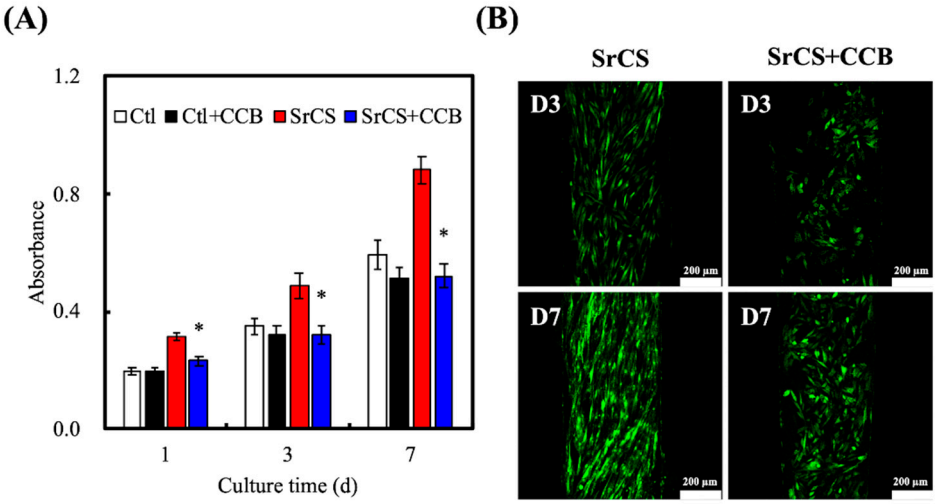

Figure 4. (**A**) Proliferation of WJMSCs on SrCS scaffolds without/with calcium channel blocker (CCB) for different time-points and (**B**) F-actin immunofluorescence staining. Data presented as mean ± SEM, $n = 6$ for each group. "*" indicates a significant difference ($p < 0.05$) when compared to substrate without CCB. Scale bar: 200 μm.

2.4. MAPK Pathway

The levels of extracellular signal-regulated protein kinase (ERK) and p38 were measured by western blot (Figure 5). As seen from the results, SrCS had higher expressions of pERK and pp38 as compared to Ctl and SrCS/CCB. Similarly, in the above studies, SrCS/CCB had lesser expressions of cell signaling proteins as compared to the rest of the groups. In addition, quantitative results showed that SrCS/CCB had significantly lower pERK/ERK and pp38/p38 ratio as compared to SrCS and Ctl. SrCS had the highest ratio as compared to the rest of the groups, which was approximately 1.4-times higher as compared to Ctl, and 3.5-times higher as compared to the SrCS/CCB group.

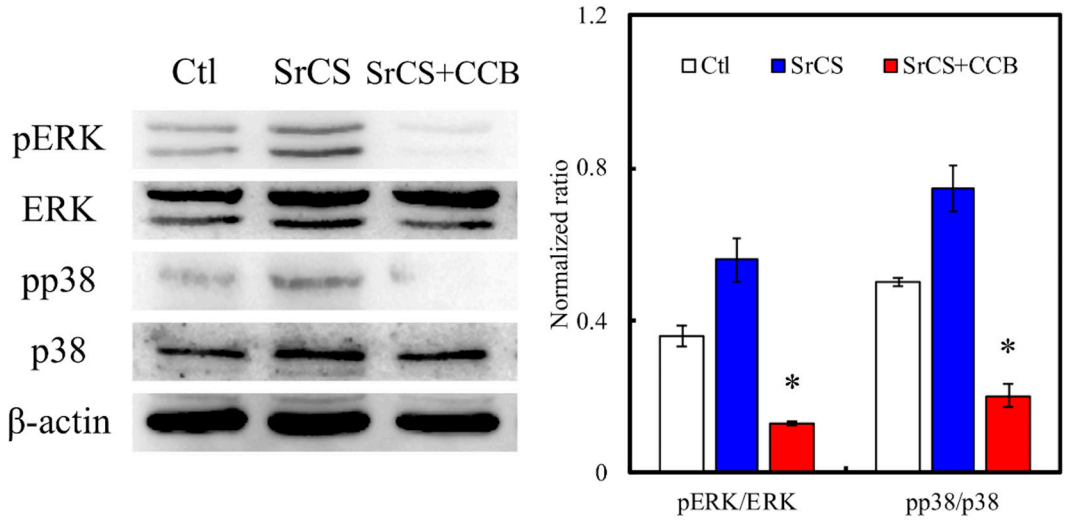

Figure 5. Western blot experiments showed the expression of ERK, p-ERK, pp38, and p38 signaling pathways proteins of WJMSCs cultured on the SrCS scaffold for 24 h. "*" indicates a significant difference ($p < 0.05$) when compared to SrCS. Data presented as mean ± SEM, $n = 3$ for each group. "Ctl" represented cells that grew in empty wells without any scaffolds.

2.5. Osteogenesis

Alkaline Phosphatase (ALP) assay results indicated that WJMSC cultured in SrCS/CCB had significantly lower levels of ALP at all time points as compared to SrCS (Figure 6). The amounts of Col I, OPN, and OC were also quantified and shown in Figure 7. It was demonstrated the SrCS/CCB group had significantly lower expressions of Col I, OPN, and OC at all time points. SrCS had approximately 0.3x and 0.7x more Col I secretions at 3 and 7 days, respectively. In addition, SrCS had 200 pg/mL of OPN secretions at day 3 as compared to 100 pg/mL for SrCS/CCB. SrCS had 3x more OPN secretions at day 7 as compared to SrCS/CCB. On the other hand, there were no noticeable statistical differences between OC secretions of both SrCS and SrCS/CCB on day 3. There were only significant differences between OC secretions of both scaffolds at day 7, whereby SrCS was found to have 2.2x higher OC secretions as compared to SrCS/CCB. In addition, SrCS was shown to have a significant 2x higher amount of ALP as compared to SrCS/CCB after both 3 and 7 days of culture. Alizarin Red S staining and quantification of Ca precipitation was conducted to consider the osteogenic capabilities of the various scaffolds (Figure 8). From Figure 8A, SrCS had a distinct darker purplish staining as compared to SrCS/CCB. Thus, this indicated that SrCS was able to induce a higher amount of Ca productions as compared to its counterpart. Especially so after 14 days of culture, there was the reddish-orange staining observed indicating high amounts of Ca deposits. On the other hand, there were only slight pinkish staining on the sides and the front of the SrCS/CCB scaffolds after 7 and 14 days of culture. In addition, quantification results of calcium secretions clearly pointed out that the SrCS scaffolds had a significantly higher amount of Ca depositions as compared to SrCS/CCB at both time points (Figure 8B). Ca quantification was approximately 4.2x higher in the SrCS group after both 7 and 14 days of culture.

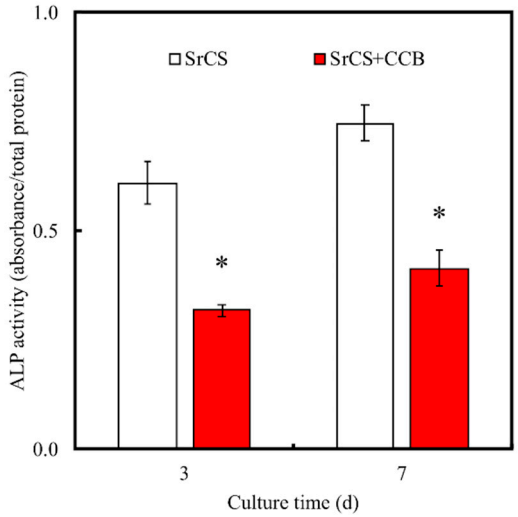

Figure 6. ALP profile of the WJMSCs cultured on the 3D-printed SrCS scaffolds in osteogenic differentiation medium without/with CCB. "*" indicates a significant difference ($p < 0.05$) when compared to SrCS.

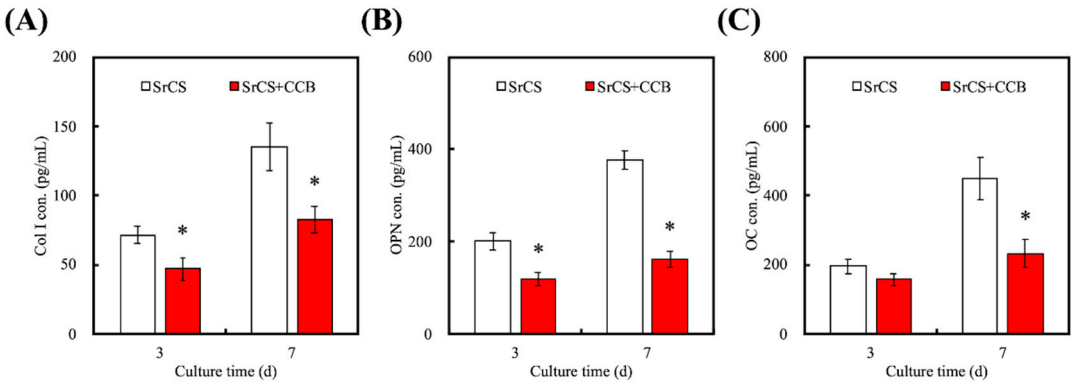

Figure 7. Proteins of (**A**) Col I, (**B**) OPN, and (**C**) OC secretion by WJMSCs were analyzed by enzyme-linked immunosorbent assay. Data presented as mean ± SEM, $n = 6$ for each group. "*" indicates a significant difference ($p < 0.05$) when compared to SrCS.

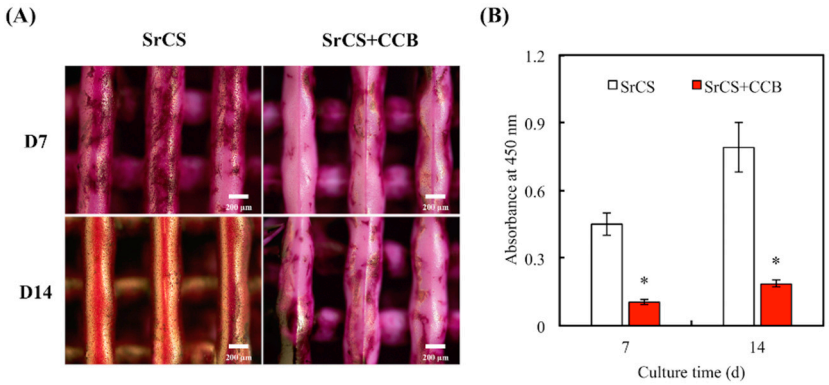

Figure 8. (**A**) Alizarin Red S staining and (**B**) quantification of Ca mineral deposits by WJMSC. Data presented as mean ± SEM, $n = 3$ for each group. "*" indicates a significant difference ($p < 0.05$) when compared to SrCS.

3. Discussion

In recent years, 3D-printing has had a huge impact on biofabrication processes as well as intelligent manufacturing for medical applications [22]. In recent years, 3D printed ceramic scaffolds have been

considered to have great potential in the application of bone tissue engineering [23,24]. It was already a known fact that CS-based materials had excellent biocompatibility and had the potential to induce apatite formation on its surface due to the reaction between Ca ions and P ions in body fluids [25]. Cell behaviors and activities were reported to be dependent and influenced by the surface chemical properties [26]. In addition, several reports had been made indicating that the addition of certain metallic elements into biomaterials may enhance bioactivity, biocompatibility, and include anti-microbial activities. Numerous modification techniques had been tested on CS such as using dopamine, aluminum alloys, or even lectins to attempt to enhance the properties of CS [27]. Previously, several studies were proved that the incorporation of additional ions, such as Mg, Zn, and Sr into the CS-based system [28–30]. We had previously reported that SrCS scaffolds can be successfully fabricated using 3D-printing techniques and that such a modified scaffold was shown to have better biological properties as compared to the traditional CS scaffolds [20]. In this study, it can be seen that Sr modification does not affect the printing quality of SrCS scaffolds, as seen by the smooth and continuous printing of the struts. Furthermore, the layers were able to be stacked during printing thus indicating that we are able to fabricate larger scaffolds if there are any requirements. It was also reported by many others that the geometry of scaffolds plays an important role in significantly enhancing cellular behaviors and activities. Current studies state that pores with a size of up to 500–750 μm were critical for bone tissue regeneration and growth. Different cell lines require different pore sizes; however, pores were found to be critical as they provide contact points for cells to adhere to, and it was further reported that efficient initial adhesion allows enhanced subsequent downstream cellular activities and behaviors, such as enhanced cellular proliferation and tissue regeneration [31].

In addition, the presence of both Sr and calcium peaks in the XRD results strongly indicated that the original compositions were still present after modification, thus showing that the modification did not affect the structural properties of CS and that the advantages of CS were still present after the modification. It was reported by others that SrCS had reduced calcium concentrations as compared to CS as Sr modification was shown to change the crystallinity of CS powder by rearranging the micro-structures of CS. Furthermore, the existence of the various Sr peaks proved the incorporation of Sr into CS [19]. Another important characteristic to note is that a good scaffold must have the capability to release ions in a steady, sustained manner in order to observe therapeutic results. Many biomaterials were noted to have initial burst release effects with the drastically reduced release over the implantation periods. In addition, the release must not be too rapid or too high to avoid having detrimental effects [14]. Similarly, it was reported by others that the sustained release of ions could lead to the formation of bone-like apatite which could then be used as a prediction of downstream osteogenic capabilities. In addition, the precipitation of such apatite layers was considered important in the fabrication of osteoconductive biomaterials for orthopedic applications [32]. Si on surfaces of scaffolds was reported to undergo changes upon contact with SBF and thus induce apatite formation. In addition, SrCS were considered hydrophilic, thus, allowing water-uptake and allow absorption of organic ions onto its surfaces. Such a property permits SrCS to have a higher amount of hydroxyapatite as compared to others [33]. As seen from the post immersion results, SrCS scaffolds were able to release Sr and Si ions onto surrounding fluids over time [34].

SrCS scaffolds were shown to enhance MSCs secretion of osteoprotegerin, able to suppress macrophage colony-stimulating factor (M-CSF) and enhance both angiogenesis and osteogenesis in in-vivo studies thus making it a promising and potential candidate for bone tissue engineering [20]. However, the underlying mechanism of SrCS and its role in enhancing cellular activities remains unknown. Local extracellular ionic changes were previously reported to have certain enhancing effects on cellular activities [35]. In this study, there was an initial burst release of Si ions from the SrCS scaffold after day 1, and eventually decreased to a gradual release for the rest of the immersion period. A study done by Valerio et al. indicated that Si ions of <2 mM were able to enhance osteoblast proliferation and collagen secretion which was also in good agreement with previous reports [36]. In addition, it was reported that Si enhances cell proliferation by promoting cellular entry into S and G2 phases of the

cell cycle. In this study, it was also seen that Sr had similar release profiles as Si ions. In this aspect, SrCS scaffolds were thus hypothesized to be able to enhance bone tissue formation and a previous study conducted by us showed enhanced osteogenesis and angiogenesis capabilities of SrCS scaffolds. In addition, it was reported that SrCS had improved anti-inflammatory capabilities as compared to CS scaffolds. There was a study made by Yang et al. stated that 0.0623 mM of Si ion was able to bring about anti-inflammatory capabilities [37]. Therefore, our initial results indicated that the ions released from SrCS scaffolds had a role to play in enhancing cellular behaviors such as cell proliferation, differentiation and even osteogenesis. Different levels of Sr were reported to having various effects and it was shown that sufficient levels of Sr ions were able to allow osteogenesis but too high levels of Sr would lead to defective bone mineralization [38].

In the present study, SrCS had shown significantly higher levels of cellular proliferation than Ctl at all time points. This result was to be expected, and it was in good agreement with reports made by others. Therefore, we used verapamil, which was a known potent inhibitor of L-type calcium channels, and it could be seen from this study that Verapamil was able to suppress the enhancement effects of Sr on WJMSCs. Interestingly, the verapamil had a profound impact on the cellular proliferation of SrCS scaffolds. SrCS/CCB had significantly lower proliferation as compared to SrCS scaffolds. However, it was noted to have higher proliferation as compared to Ctl/CCB. The immunofluorescence results from Figure 4B supported the fact that verapamil was indeed able to decrease proliferation. Cells treated with verapamil were rounded and had lesser cytoplasmic protrusions as compared to SrCS specimens [39]. Such an observation indicated that cells were not properly adhered to the surfaces of scaffolds. It was reported by others that the degree of initial adhesion could be used as a predictive indicator for assessing subsequent downstream cellular behaviors [40]. There were several studies demonstrated the mechanism by Si affect cell behavior is not fully understood at present; the MAPK/ERK and MAPK/p38 pathways have been suggested been the important factor in facilitating cell proliferation and differentiation [41]. MAPK-related pathways are important mediators of biological behaviors to extracellular factors effects [42]. Moreover, we had proved the CS-based materials treated with verapamil, a type of L-type calcium channel inhibitor, exhibited down-regulation effects of Si-induced ERK and p38 phosphorylation [43]. CS-based materials were able to enhance cellular proliferation and activities via increasing Si ion influx through L-type calcium channels, thus leading to enhanced activation of ERK and p38 MAPK pathways which led to subsequent up-regulated cellular activities. Some studies indicated the calcium-sensing receptor (CaR) is the important receptor involved in Sr-regulated proliferation and differentiation of primary cells [44].

The levels of ALP and calcium mineralization were subsequently measured to determine the effects of verapamil on osteogenic capabilities of SrCS scaffolds. As seen from the results, verapamil was able to reduce ALP secretion significantly as compared to SrCS. ALP is considered a crucial protein present during the early stages of osteogenesis, where the stem cells are starting to differentiate into osteoblasts. Therefore, ALP can be used as an early marker for osteogenesis. The present result demonstrated that blocking the Ca channel by treatment with verapamil reduces SrCS-induced osteogenic differentiation in WJMSCs [43]. Col I, OPN, and OC are common markers used for evaluating osteogenesis. OC is different from ALP in the sense that it is a non-collagenous protein hormone that is secreted by osteoblasts. Furthermore, ALP was commonly reported to be involved in early mineralization processes with its level peaking during the early bone formation phases whilst Col I is mostly found in the cellular proliferative and ECM secretion stage. OC is another common market used for evaluating osteogenesis. However, OC is usually found in the last few stages of osteogenesis, whereby its role is to bind to extracellular calcium ions for further bone development. From this study, it can be seen that verapamil was able to reduce these protein expressions and secretions significantly. These results were similar to that of Wu [45], who proved that Si up-regulated the protein expression of ALP, CEMP1, and RUNX2 in primary cells. In addition, Sr ions can activate Ca sensing receptors and promote osteogenic-related protein production [46]. They also suggested the Sr-induced osteogenesis differentiation is affected via the Wnt signaling pathway [47]. Furthermore, Ca mineralization was significantly reduced as

seen from the Alizarin red S staining and quantification test. These results were in good agreement with each other by suggesting that verapamil was able to inhibit cellular proliferation thus leading to decreased differentiation of WJMSC into osteoblasts and reduced Ca mineralization on the SrCS scaffold. Based on these findings, we presume that an influx via the Ca channel and intracellular accumulation of SrCS trigger the signaling incidents and activating downstream ERK/MAPK pathways leading to allow WJMSC differentiated to osteoblasts.

4. Materials and Methods

4.1. SrCS Scaffold Fabrication

SrCS powders were synthesized with methods, as published previously [20]. Commercially proven analytically graded reagents were purchased from Sigma-Aldrich (Sigma-Aldrich, St. Louis, MO, USA). 65% calcium oxide (CaO) was mixed with 20% silicon dioxide (SiO2), 10% strontium oxide (SrO), and 5% alumina oxide (Al2O3), subsequently sintered at 1400 °C for 2 h and cooled to room temperature. The mixtures were placed into 99.5% ethanol and further ground with agate milling balls in a planetary ball mill machine (Retsch PM-100, Retsch GmbH, Germany) for 12 h. Then, the mixture was dried at 100 °C in an oven for 12 h.

In this study, SrCS powder was mixed with polycaprolactone (PCL, Mw = 43,000–50,000, Polysciences, Warrington, PA, USA) by first stirring it in ethanol with melted PCL at 200 °C was slowly dropped into the solution. The solution was then continuously stirred until the ethanol had evaporated. Next, the injectable mixture was transferred into new 20 mL cartridges and placed onto the BioScaffolder (BioScaffolder 3.1, GeSiM, Großerkmannsdorf, Germany). The design of the scaffold was drafted using a built-in software with a line width of 500 μm, printed via a 400 μm needle, with 300 kPa applied pressure and a printing speed of 2 mm/s. The composition of the SrCS scaffold was analyzed using X-ray diffractometry (XRD; Bruker D8 SSS, Karlsruhe, Germany). Diffraction pattern of the scaffolds was conducted using X-ray diffraction with the following parameters: 2θ from 20° to 50° s with scanning steps of 1°/min.

4.2. Apatite Precipitate

The printed SrCS scaffolds were sterilized using absolute ethanol prior to cell culture. The scaffolds were then dried and placed into a clean centrifuge tube and filled with simulated body fluid (SBF). The SBF solution has a similar ionic composition to human blood plasma and was made up of 7.9949 g of NaCl, 0.3528 g of NaHCO3, 0.2235 g of KCl, 0.147 g of K2HPO4, 0.305 g of MgCl2·6H2O, 0.2775 g of CaCl2, and 0.071 of g Na2SO4 in 1000 mL of distilled water. The centrifuge tubes were then sealed and placed into a shaker at 37 °C for various durations. After different durations of immersion, the scaffolds were then removed from the tube and examined using SEM to observe for the morphology of the hydroxyapatite formation on the surfaces of the scaffolds. Ca, Si and Sr ions in the solution was examined using an inductive coupled plasma-atomic emission spectrometer (ICP-AES; Perkin-Elmer OPT 1MA 3000DV, Shelton, CT, USA).

4.3. Cell Proliferation

The human Wharton's jelly mesenchymal stem cells (WJMSCs) used in this study were obtained from the Bioresource Collection and Research Center (BCRC, Hsin-Chu, Taiwan). The WJMSCs were incubated in the following settings: 37 °C, 5% CO2/95% air and mesenchymal stem cell medium (#7501, Sciencell, Carlsbad, CA, USA) to passage 3-6. Similarly, prior to any in vitro tests, the scaffolds were sterilized using 75% ethanol and UV exposure for 30 min. Cell suspensions of 5 × 104 cells/per scaffold were seeded onto the scaffolds and PrestoBlue™ (Invitrogen, Grand Island, NY, USA) was used to assess for cellular proliferation according to the manufacturer's instructions. In short, the scaffolds were removed, washed thrice with cold PBS and placed into fresh microplates. 30 μL of PrestoBlue solution and 270 μL of DMEM were mixed, pipetted into each well and incubated for 1 h. Then, 100 μL

from each well was pipetted to a fresh 96-well microplate. The absorbance of each well was determined using a Tecan Infinite 200® PRO microplate reader (Tecan, Männedorf, Switzerland) at a wavelength of 570 nm and 600 nm reference wavelength. Cells cultured on culture plates without scaffolds were used as controls (Ctl). The culture medium was mixed with 5 μM Verapamil for SrCS/CCB groups.

In addition, fluorescence staining was used to observe cellular morphology. After culture, the cells and scaffolds were washed with PBS and fixed in 4% paraformaldehyde (Sigma-Aldrich) solution for 20 min at room temperature. Next, the cells were permeabilized using 0.1% Triton X-100 (Sigma-Aldrich) and the F-actin cytoskeleton was stained with fluorescent dye Alexa Fluor 488 (Invitrogen) conjugated to phalloidin to observe for morphology and cellular distribution. Then, the specimens were rinsing using PBS several times, and the cell morphology of WJMSCs was examined using Leica TCS SP8 X white light laser confocal microscope (Leica Microsystems GmbH, Wetzlar, Hessen, Germany).

4.4. Western Blot

After 24 h of culture, cells were lysed using NP40 buffer (Thermo Fisher), and a BCA protein assay kit was used to assess for protein concentrations. The cell lysates (30 μg protein) were separated using SDS-polyacrylamide gel electrophoresis and transferred to nitrocellulose membranes. Bovine serum albumin (BSA, Sigma-Aldrich), at a concentration of 5%, was used to incubate for 1 h and the membrane was immunoblotted with primary anti-ERK1/2, anti-phospho-ERK1/2, anti-p38, anti-phospho-p38 and anti-β-actin antibodies (Abcam, Cambridge, MA, USA) for 2 h. It was then washed three times using tris-buffer saline with 0.05% Tween-20 (Sigma-Aldrich). Horseradish peroxidase (HRP)-conjugated secondary antibody was then added and the proteins were assessed using enhanced chemiluminescent detection kits (Invitrogen). The stained bands were then scanned, quantified using a densitometer (Syngene bioimaging system; Frederick, MD) and ImageJ (National Institutes of Health, Bethesda, MD) normalized to β-actin. The results were obtained in triplicate from three separate samples for each test.

4.5. ALP Activity

ALP levels were determined by first culturing cells on 3D-printed SrCS scaffold with an osteogenic medium for 3 and 7 days (StemPro™ osteogenesis differentiation kit, Invitrogen). Cells were then lysed with 0.2% NP-40, rinsed with PBS, and centrifuged at 2000 rpm for 10 min. p-nitrophenyl phosphate (pNPP, Sigma) was used to determine the levels of ALP activity. pNPP was first mixed with 1 M diethanolamine buffer and the samples were immersed for 15 min. NaOH (5 N) was used to terminate the reactions and ALP was quantified using a 405 nm spectrophotometer. All data were normalized to data obtained from a BCS protein assay kit with BSA as the standard.

4.6. Osteogenic-Related Protein

WJMSCs were cultured on the 3D-printed SrCS scaffolds and for 3 and 7 days and lysed using the methods above. Collagen I (Col I), osteopontin (OPN), and osteocalcin (OC) protein concentration were measured using an enzyme-linked immunosorbent assay kit (Abcam) and conducted according to manufacturer's instructions with reference to the standard curve. For this study, the blank wells were used as Ctl, and the tests were conducted in triplicates and tabulated from 6 independent tests.

4.7. Mineralization

After 7 and 14 days of culture, calcium mineralization from WJMSC was measured using alizarin red S staining. The level of mineralization was considered after the cells were seeded on the 3D-printed SrCS scaffold and cultured with the osteogenic medium. After that, the samples were immersed in 4% paraformaldehyde (Sigma-Aldrich) for 20 min and 0.5% alizarin red S (pH 4.0, Sigma-Aldrich) was then added and incubated for 20 min at room temperature in the dark. The cells were then washed with PBS solution and the alizarin red S staining was chelates with 20% methanol and 10% acetic acid for 15 min. The solution was then transferred to a 96-well plate quantified using a Tecan Infinite 200® PRO microplate reader at 450 nm.

4.8. Statistical Analysis

One-way variance statistical analysis was used to assess significant differences in each group, and Scheffe's multiple comparison test was used for each specimen. $P < 0.05$ was considered statistically significant.

5. Conclusions

In summary, the 3D-printed SrCS scaffold was proven to be able to enhance cell proliferation and to influence the promising mechanism of differentiation towards an osteogenic phenotype. The current study was demonstrated the new and important clues considering the molecular mechanisms that 3D-printed SrCS scaffold-stimulated osteogenesis differentiation in WJMSCs, and was regulated by the influx of extracellular ions via the Ca channel and activated of ERK/MAPK pathway. Moreover, our results support that Ca channel blockers could potentially have depressed the proliferation, differentiation, and mineralization of WJMSC when SrCS scaffolds were used. Moreover, the 3D-printed SrCS scaffolds possess the osteoinductivity bone substitute because of the synergetic effect of Si and Sr ions. Therefore, we can infer that 3D-printed SrCS scaffolds are an ideal bone tissue regeneration graft that has promising applications in orthopedic surgery.

Author Contributions: Data Curation, T.-R.S.; Formal Analysis, H.Y.N.; Funding Acquisition, T.-R.S. and T.-T.H.; Investigation, T.-R.S.; Methodology, C.-T.K.; Writing—Original Draft, T.-H.H. and H.Y.N.; Writing—Review and Editing, Y.-C.C. and T.-T.H. All authors have read and agreed to the published version of the manuscript.

Funding: The authors acknowledge receipt grants from the Ministry of Science and Technology (MOST 106-2314-B-040-003-MY3 and 108-2314-B-039-041), Antai Medical Care Cooperation Antai Tian-Sheng Memorial Hospital and Chung Shan Medical University (CSMU-TSMH-106-02), and the China Medical University Hospital grants (DMR-109-079).

Acknowledgments: Experiments and data analysis were performed in part through the use of the Medical Research Core Facilities Center, Office of Research and Development at the China Medical University. SEM image was assisted by Ya-Hsun Lin (MOST 108-2731-M-005-001).

Conflicts of Interest: The authors declare no conflict of interest.

References

1. Rodriguez-Palomo, A.; Monopoli, D.; Afonso, H.; Izquierdo-Barba, I.; Vallet-Regí, M. Surface zwitterionization of customized 3D Ti6Al4V scaffolds: A promising alternative to eradicate bone infection. *J. Mater. Chem. B* **2016**, *4*, 4356–4365. [CrossRef]
2. Shim, J.H.; Won, J.Y.; Park, J.H.; Bae, J.H.; Ahn, G.; Kim, C.H.; Lim, D.H.; Cho, D.W.; Yun, W.S.; Bae, E.B.; et al. Effects of 3D-printed polycaprolactone/β-tricalcium phosphate membranes on guided bone regeneration. *Int. J. Mol. Sci.* **2017**, *18*, 899. [CrossRef]
3. Xia, Y.; Guo, Y.; Yang, Z.; Chen, H.; Ren, K.; Weir, M.D.; Chow, L.C.; Reynolds, M.A.; Zhang, F.; Gu, N.; et al. Iron oxide nanoparticle-calcium phosphate cement enhanced the osteogenic activities of stem cells through WNT/β-catenin signaling. *Mater. Sci. Eng. C Mater. Biol. Appl.* **2019**, *104*, 109955. [CrossRef]
4. Gandolfi, M.G.; Zamparini, F.; Degli Esposti, M.; Chiellini, F.; Aparicio, C.; Fava, F.; Fabbri, P.; Taddei, P.; Prati, C. Polylactic acid-based porous scaffolds doped with calcium silicate and dicalcium phosphate dihydrate designed for biomedical application. *Mater. Sci. Eng. C Mater. Biol. Appl.* **2018**, *82*, 163–181. [CrossRef]
5. Park, S.; Lee, H.J.; Kim, K.S.; Lee, S.; Lee, J.T.; Kim, S.Y.; Chang, N.H.; Park, S.Y. In vivo evaluation of 3D-printed polycaprolactone scaffold implantation combined with β-TCP powder for alveolar bone augmentation in a beagle defect model. *Materials* **2018**, *11*, 238. [CrossRef]
6. Lee, H.; Yang, G.H.; Kim, M.; Lee, J.; Huh, J.; Kim, G. Fabrication of micro/nanoporous collagen/dECM/silk-fibroin biocomposite scaffolds using a low temperature 3D printing process for bone tissue regeneration. *Mater. Sci. Eng. C Mater. Biol. Appl.* **2018**, *84*, 140–147. [CrossRef]
7. Shao, H.; Ke, X.; Liu, A.; Sun, M.; He, Y.; Yang, X.; Fu, J.; Liu, Y.; Zhang, L.; Yang, G.; et al. Bone regeneration in 3D printing bioactive ceramic scaffolds with improved tissue/material interface pore architecture in thin-wall bone defect. *Biofabrication* **2017**, *9*, 025003. [CrossRef]

8. Kao, C.T.; Lin, C.C.; Chen, Y.W.; Yeh, C.H.; Fang, H.Y.; Shie, M.Y. Poly(dopamine) coating of 3D printed poly(lactic acid) scaffolds for bone tissue engineering. *Mater. Sci. Eng. C Mater. Biol. Appl.* **2015**, *56*, 165–173. [CrossRef]
9. Hollister, S.J. Scaffold design and manufacturing: From concept to clinic. *Adv. Mater* **2009**, *21*, 3330–3342. [CrossRef] [PubMed]
10. Wu, Y.H.; Chiu, Y.C.; Lin, Y.H.; Ho, C.C.; Shie, M.Y.; Chen, Y.W. 3D-printed bioactive calcium silicate/poly-ε-caprolactone bioscaffolds modified with biomimetic extracellular matrices for bone regeneration. *Int. J. Mol. Sci.* **2019**, *20*, 942. [CrossRef] [PubMed]
11. Lin, Y.H.; Chuang, T.Y.; Chiang, W.H.; Chen, I.W.P.; Wang, K.; Shie, M.Y.; Chen, Y.W. The synergistic effects of graphene-contained 3D-printed calcium silicate/poly-ε-caprolactone scaffolds promote FGFR-induced osteogenic/angiogenic differentiation of mesenchymal stem cells. *Mater. Sci. Eng. C Mater. Biol. Appl.* **2019**, *104*, 109887. [CrossRef]
12. Chen, Y.W.; Hsu, T.T.; Wang, K.; Shie, M.Y. Preparation of the fast setting and degrading Ca-Si-Mg cement with both odontogenesis and angiogenesis differentiation of human periodontal ligament cells. *Mater. Sci. Eng. C Mater. Biol. Appl.* **2016**, *60*, 374–383. [CrossRef] [PubMed]
13. Hao, F.; Qin, L.; Liu, J.; Chang, J.; Huan, Z.; Wu, L. Assessment of calcium sulfate hemihydrate–tricalcium silicate composite for bone healing in a rabbit femoral condyle model. *Mater Sci. Eng. C Mater. Biol. Appl.* **2018**, *88*, 53–60. [CrossRef] [PubMed]
14. Shie, M.Y.; Ding, S.J.; Chang, H.C. The role of silicon in osteoblast-like cell proliferation and apoptosis. *Acta Biomater.* **2011**, *7*, 2604–2614. [CrossRef] [PubMed]
15. Shie, M.Y.; Ding, S.J. Integrin binding and MAPK signal pathways in primary cell responses to surface chemistry of calcium silicate cements. *Biomaterials* **2013**, *34*, 6589–6606. [CrossRef]
16. Shie, M.Y.; Chiang, W.H.; Chen, I.W.P.; Liu, W.Y.; Chen, Y.W. Synergistic acceleration in the osteogenic and angiogenic differentiation of human mesenchymal stem cells by calcium silicate–graphene composites. *Mater. Sci. Eng. C Mater. Biol. Appl.* **2017**, *73*, 726–735. [CrossRef]
17. Liu, L.; Liu, Y.; Feng, C.; Chang, J.; Fu, R.; Wu, T.; Yu, F.; Wang, X.; Xia, L.; Wu, C.; et al. Lithium-containing biomaterials stimulate bone marrow stromal cell-derived exosomal miR-130a secretion to promote angiogenesis. *Biomaterials* **2018**, *192*, 523–536. [CrossRef]
18. Ke, D.; Tarafder, S.; Vahabzadeh, S.; Bose, S. Effects of MgO, ZnO, SrO, and SiO2 in tricalcium phosphate scaffolds on in vitro gene expression and in vivo osteogenesis. *Mater. Sci. Eng. C Mater. Biol. Appl.* **2019**, *96*, 10–19. [CrossRef]
19. Huang, T.H.; Kao, C.T.; Shen, Y.F.; Lin, Y.T.; Liu, Y.T.; Yen, S.Y.; Ho, C.C. Substitutions of strontium in bioactive calcium silicate bone cements stimulate osteogenic differentiation in human mesenchymal stem cells. *J. Mater. Sci.: Mater. Med.* **2019**, *30*, 68. [CrossRef]
20. Chiu, Y.C.; Shie, M.Y.; Lin, Y.H.; Lee, K.X.; Chen, Y.W. Effect of strontium substitution on the physicochemical properties and bone regeneration potential of 3D printed calcium silicate scaffolds. *Int. J. Mol. Sci.* **2019**, *20*, 2729. [CrossRef]
21. Quade, M.; Schumacher, M.; Bernhardt, A.; Lode, A.; Kampschulte, M.; Voß, A.; Simon, P.; Uckermann, O.; Kirsch, M.; Gelinsky, M. Strontium-modification of porous scaffolds from mineralized collagen for potential use in bone defect therapy. *Mater. Sci. Eng. C Mater. Biol. Appl.* **2018**, *84*, 159–167. [CrossRef] [PubMed]
22. Shie, M.Y.; Shen, Y.F.; Astuti, S.D.; Lee, K.X.; Lin, S.H.; Dwijaksara, N.L.B.; Chen, Y.W. Review of polymeric materials in 4D printing biomedical applications. *Polymers* **2019**, *11*, 1864. [CrossRef] [PubMed]
23. Huang, K.H.; Lin, Y.H.; Shie, M.Y.; Lin, C.P. Effects of bone morphogenic protein-2 loaded on the 3D-printed MesoCS scaffolds. *J. Formos. Med. Assoc.* **2018**, *117*, 879–887. [CrossRef] [PubMed]
24. Tamburaci, S.; Tihminlioglu, F. Biosilica incorporated 3D porous scaffolds for bone tissue engineering applications. *Mater. Sci. Eng. C Mater. Biol. Appl.* **2018**, *91*, 274–291. [CrossRef] [PubMed]
25. Huang, K.H.; Chen, Y.W.; Wang, C.Y.; Lin, Y.H.; Wu, Y.H.; Shie, M.Y.; Lin, C.P. Enhanced capability of BMP-2-loaded mesoporous calcium silicate scaffolds to induce odontogenic differentiation of human dental pulp cells. *J. Endod.* **2018**, *44*, 1677–1685. [CrossRef] [PubMed]
26. Garcia-Cruz, A.; Lee, M.; Zine, N.; Sigaud, M.; Marote, P.; Lopez, M.; Bausells, J.; Jaffrézic-Renault, N.; Errachid, A. Biopatterning of antibodies on poly(pyrrole)-nanowires using nanocontact printing: Surface characterization. *Mater. Sci. Eng. C Mater. Biol. Appl.* **2018**, *91*, 466–474. [CrossRef]

27. Kao, C.T.; Chen, Y.J.; Ng, H.Y.; Lee, K.X.; Huang, T.H.; Lin, T.F.; Hsu, T.T. Surface modification of calcium silicate via mussel-inspired polydopamine and effective adsorption of extracellular matrix to promote osteogenesis differentiation for bone tissue engineering. *Materials* **2018**, *11*, 1664. [CrossRef]
28. Zhu, Y.; Zhu, M.; He, X.; Zhang, J.; Tao, C. Substitutions of strontium in mesoporous calcium silicate and their physicochemical and biological properties. *Acta Biomater.* **2013**, *9*, 6723–6731. [CrossRef]
29. Chen, Y.W.; Yeh, C.H.; Shie, M.Y. Stimulatory effects of the fast setting and degradable Ca–Si–Mg cement on both cementogenesis and angiogenesis differentiation of human periodontal ligament cells. *J. Mater. Chem. B* **2015**, *3*, 7099–7108. [CrossRef]
30. Wu, C.; Miron, R.; Sculean, A.; Kaskel, S.; Doert, T.; Schulze, R.; Zhang, Y. Proliferation, differentiation and gene expression of osteoblasts in boron-containing associated with dexamethasone deliver from mesoporous bioactive glass scaffolds. *Biomaterials* **2011**, *32*, 7068–7078. [CrossRef]
31. Chiu, Y.C.; Shen, Y.F.; Lee, K.X.; Lin, S.H.; Wu, Y.C.; Chen, Y.W. 3D printing of amino resin-based photosensitive materials on multi-parameter optimization design for vascular engineering applications. *Polymers* **2019**, *11*, 1394. [CrossRef]
32. Yu, Q.; Chang, J.; Wu, C. Silicate bioceramics: From soft tissue regeneration to tumor therapy. *J. Mater. Chem. B* **2019**, *7*, 5449–5460. [CrossRef]
33. Roohaniesfahani, I.; Wang, J.; No, Y.J.; de Candia, C.; Miao, X.; Lu, Z.; Shi, J.; Kaplan, D.L.; Jiang, X.; Zreiqat, H. Modulatory effect of simultaneously released magnesium, strontium, and silicon ions on injectable silk hydrogels for bone regeneration. *Mater. Sci. Eng. C Mater. Biol. Appl.* **2019**, *94*, 976–987. [CrossRef]
34. Liu, W.C.; Hu, C.C.; Tseng, Y.Y.; Sakthivel, R.; Fan, K.-S.; Wang, A.N.; Wang, Y.M.; Chung, R.J. Study on strontium doped tricalcium silicate synthesized through sol-gel process. *Mater. Sci. Eng. C Mater. Biol. Appl.* **2020**, *108*, 110431. [CrossRef]
35. Zhai, D.; Xu, M.; Liu, L.; Chang, J.; Wu, C. Silicate-based bioceramics regulating osteoblast differentiation through a BMP2 signalling pathway. *J. Mater. Chem. B* **2017**, *5*, 7297–7306. [CrossRef]
36. Valerio, P.; Pereira, M.M.; Goes, A.M.; Leite, M.F. The effect of ionic products from bioactive glass dissolution on osteoblast proliferation and collagen production. *Biomaterials* **2004**, *25*, 2941–2948. [CrossRef]
37. Yang, C.; Wang, X.; Ma, B.; Zhu, H.; Huan, Z.; Ma, N.; Wu, C.; Chang, J. 3D-printed bioactive Ca3SiO5 bone cement scaffolds with nano surface structure for bone regeneration. *ACS Appl. Mater Interfaces* **2017**, *9*, 5757–5767. [CrossRef]
38. Prabha, R.D.; Nair, B.P.; Ditzel, N.; Kjems, J.; Nair, P.D.; Kassem, M. Strontium functionalized scaffold for bone tissue engineering. *Mater Sci. Eng. C Mater Biol. Appl.* **2019**, *94*, 509–515. [CrossRef]
39. Touil, Y.; Zuliani, T.; Wolowczuk, I.; Kuranda, K.; Prochazkova, J.; Andrieux, J.; Le Roy, H.; Mortier, L.; Vandomme, J.; Jouy, N.; et al. The PI3K/AKT signaling pathway controls the quiescence of the low-rhodamine123-retention cell compartment enriched for melanoma stem cell activity. *Stem. Cells* **2013**, *31*, 641–651. [CrossRef]
40. Zahanich, I.; Graf, E.M.; Heubach, J.F.; Hempel, U.; Boxberger, S.; Ravens, U. Molecular and functional expression of voltage-operated calcium channels during osteogenic differentiation of human mesenchymal stem cells. *J. Bone Miner Res.* **2005**, *20*, 1637–1646. [CrossRef]
41. Wu, C.; Han, P.; Xu, M.; Zhang, X.; Zhou, Y.; Xue, G.; Chang, J.; Xiao, Y. Nagelschmidtite bioceramics with osteostimulation properties: Material chemistry activating osteogenic genes and WNT signalling pathway of human bone marrow stromal cells. *J. Mater. Chem. B* **2013**, *1*, 876–885. [CrossRef]
42. Woo, S.M.; Hwang, Y.C.; Lim, H.S.; Choi, N.K.; Kim, S.H.; Kim, W.J.; Kim, S.M.; Jung, J.Y. Effect of nifedipine on the differentiation of human dental pulp cells cultured with mineral trioxide aggregate. *J. Endod.* **2013**, *39*, 801–805. [CrossRef] [PubMed]
43. Wu, B.C.; Kao, C.T.; Huang, T.H.; Hung, C.J.; Shie, M.Y.; Chung, H.Y. Effect of verapamil, a calcium channel blocker, on the odontogenic activity of human dental pulp cells cultured with silicate-based materials. *J. Endod.* **2014**, *40*, 1105–1111. [CrossRef] [PubMed]
44. Yang, F.; Yang, D.; Tu, J.; Zheng, Q.; Cai, L.; Wang, L. Strontium enhances osteogenic differentiation of mesenchymal stem cells and in vivo bone formation by activating Wnt/catenin signaling. *Stem. Cells* **2011**, *29*, 981–991. [CrossRef]
45. Wu, C.; Zhou, Y.Z.; Lin, C.; Chang, J.; Xiao, Y. Strontium-containing mesoporous bioactive glass scaffolds with improved osteogenic/cementogenic differentiation of periodontal ligament cells for periodontal tissue engineering. *Acta Biomater.* **2012**, *8*, 3805–3815. [CrossRef]

46. Lei, Y.; Xu, Z.; Ke, Q.; Yin, W.; Chen, Y.; Zhang, C.; Guo, Y. Strontium hydroxyapatite/chitosan nanohybrid scaffolds with enhanced osteoinductivity for bone tissue engineering. *Mater. Sci. Eng. C Mater. Biol. Appl.* **2017**, *72*, 134–142. [CrossRef]
47. Fielding, G.A.; Smoot, W.; Bose, S. Effects of SiO2, SrO, MgO, and ZnO dopants in tricalcium phosphates on osteoblastic Runx2 expression. *J. Biomed. Mater. Res. Part A* **2014**, *102*, 2417–2426. [CrossRef]